

## Induced weak currents and $\beta^\pm$ - $\alpha$ angular correlations in $A = 8^\dagger$

R. E. Tribble\* and G. T. Garvey

*Joseph Henry Laboratories, Princeton University, Princeton, New Jersey 08540*

(Received 20 February 1975)

$\beta$ - $\alpha$  angular correlations of the form  $\omega(\theta_{\beta\alpha}) = 1 + a \cos\theta_{\beta\alpha} + p \cos^2\theta_{\beta\alpha}$  have been measured as a function of  $\beta$  energy for the two decays  ${}^8\text{Li} \xrightarrow{\beta^-} {}^8\text{Be} \rightarrow 2\alpha$  and  ${}^8\text{B} \xrightarrow{\beta^+} {}^8\text{Be} \rightarrow 2\alpha$ . The results of the angular correlations are considered in a model independent analysis, along with a comparison to model dependent wave function calculations. The  $a$  coefficient is a kinematic term that depends on  $(1/v^*)$ , where  $v^*$  is the center of mass velocity of the  $\alpha$  particle. A detailed comparison between the experimental results and the theoretical prediction for  $a$  shows that the measured kinematic term is (10-15)% smaller than the prediction. The  $p$  coefficients arise from induced weak currents. Utilizing the  $G$ -parity properties of these currents, we discuss the results corresponding to  $\delta_\pm = p_{\delta_{\text{Li}}} \pm p_{\delta_{\text{B}}}$ . The second order  $\beta$  energy dependence in  $\delta_-$  is found to be negligible. Assuming no second order energy dependence, the experimental result is  $(\delta_-)m_n/E_\beta = 7.0 \pm 0.5 = (b/Ac) - (d_{\text{II}}/Ac)$ , where  $b$  and  $d_{\text{II}}$  are the weak magnetism and second class currents, and  $c$  is the Gamow-Teller current. The experimental result for  $(\delta_+)m_n/E_\beta$  determines the first class induced tensor current  $d_{\text{I}}$ , and the second forbidden axial currents  $j_2$  and  $j_3$ . The interpretation of  $(\delta_+)m_n/E_\beta$  is complicated since wave function predictions indicate that all three currents should contribute significantly to  $\delta_+$ .

[ RADIOACTIVITY  ${}^8\text{Li}$ ,  ${}^8\text{B}$ ; measured  $\beta\alpha$  angular correlations. Deduced induced weak currents. ]

### I. INTRODUCTION

Even though one is quite certain of the  $V-A$  nature of the charge changing weak interaction, interesting and fundamental questions remain to be answered about semileptonic decays in recoil order. The two most fundamental points to be investigated involve the correctness of the conserved vector current (CVC) hypothesis and whether or not second class currents exist. Assuming all form factors to be of order unity, these recoil order effects are of a size  $E_L/mc^2$  where  $E_L$  is the maximum lepton energy in the decay and  $m$  is the mass of the hadron system. In nuclear  $\beta$  decay these recoil order effects are, at most, a few percent of the momentum independent terms, so any useful study of these effects involves careful, difficult experiments as well as a complete theory which considers all possible higher order processes that could affect the interpretation of a given experiment.

The number of nuclear  $\beta$  decay experiments performed to date which are sensitive to recoil order effects is quite small. In the early 1960's there was a flurry of activity in nuclear investigations of the "weak magnetism" predictions of the CVC hypothesis.

The most convincing experimental demonstration of the weak magnetism prediction of CVC was the study of the  $A=12$  spectral shape done by Lee, Mo, and Wu who substantiated the CVC hypothesis to about 30%.<sup>1</sup> The next flurry of activity in nuclear physics involving studies of induced weak currents

was in the early 1970's when Wilkinson pointed out that the observed asymmetry in the intrinsic rates in  $\beta$  decays could be attributed to a "second class" axial vector interaction.<sup>2</sup> It is now apparent that no conclusion can be drawn with regard to the size of second class currents from mirror  $ft$  asymmetries because of the effects of the Coulomb field on the decay rate.<sup>3</sup>

As a direct result of this activity, Treiman and Holstein initiated a study<sup>4</sup> of the possible directional correlation experiments that could be employed to establish a model independent basis for the determination of the size of second class currents. This work has been extended by Holstein, who in a recent review paper,<sup>5</sup> has laid out a rather complete theory of the possible correlation effects that can be detected through second order in the recoil (i.e., order  $q^2R^2$ ). These results are model independent with the nucleus being treated as an elementary particle and the unknown ratio expressed in terms of form factors to be fixed by experiment. After a careful study of the possible cases, we chose to measure the  $\beta_+-\alpha$  and  $\beta_--\alpha$  angular correlations as a function of  $\beta$  energy in the  $A=8$  system.

The relevant facts surrounding the decays are

$${}^8\text{Li} \rightarrow {}^8\text{Be}^*(2^+, 2.90) + e^- + \bar{\nu}, \quad t_{1/2} = 842 \text{ msec},$$

$$\quad \quad \quad \downarrow \alpha + \alpha$$

and

$${}^8\text{B} \rightarrow {}^8\text{Be}^*(2^+, 2.90) + e^+ + \nu, \quad t_{1/2} = 769 \text{ msec}.$$

$$\quad \quad \quad \downarrow \alpha + \alpha$$

A diagram of the  $A=8$  energy levels is shown in Fig. 1. The decays of  ${}^8\text{Li}$  and  ${}^8\text{B}$  occur between  $2^+$ ,  $T=1$  and  $2^+$ ,  $T=0$  levels, and are therefore allowed axial-vector transitions. The relatively high decay energies, in this case, enhance recoil order effects on the  $\beta$  spectra since these contributions depend upon the momentum transferred to the nucleus.

Several  $\beta$  decay experiments have been performed in the mass 8 system, including measurements of (1)  ${}^8\text{Li}$  spectrum shape,<sup>6</sup> (2)  $\log ft$  for  ${}^8\text{Li}$  and  ${}^8\text{B}$ ,<sup>7</sup> (3) energy dependence of the  $ft$  asymmetry,<sup>8</sup> (4)  ${}^8\text{Li}$   $\beta$ -neutrino  $\alpha$  angular correlation,<sup>9,10</sup> (5)  ${}^8\text{Li}$   $\beta$  asymmetry,<sup>11</sup> and (6)  ${}^8\text{Li}$  and  ${}^8\text{B}$   $\beta$ - $\alpha$  angular correlation.<sup>10,12</sup> The spectrum shape, measured via a magnetic spectrometer provided energy calibrations for the  $\beta$  spectrum measured in the present work (see Sec. III). The experimental results for the other measurements are summarized in Table I. The results for the  $\beta$ -neutrino- $\alpha$  angular correlations are consistent with  $(M_F)^2/(M_{GT})^2 < 0.05$  where  $M_F$  and  $M_{GT}$  are the Fermi and Gamow-Teller matrix elements, respectively. The likely Fermi admixture is much smaller than this limit and should be the order of 40 times smaller than this number. Negligible Fermi admixture to the decay was corroborated by the measurement of the  $\beta$  asymmetry.

## II. INDUCED CURRENTS AND THE PREDICTED ANGULAR CORRELATION

As was pointed out above, the theoretical form for the  $\beta$ - $\alpha$  angular correlation has been calculated by Holstein and Treiman, and extended by Holstein to include both recoil order contributions and contributions second order in  $(qR)$ . The transition probability is

$$dw = \frac{F(Z, E)}{(2\pi)^5} |T|^2 \delta^4(p_1 - p_2 - p - k) d^3p_2 d^3p d^3k, \quad (1)$$

where  $p_1$ ,  $p_2$ ,  $p$ , and  $k$  are the four-momenta of the parent, daughter, electron, and neutrino, respectively.  $F(Z, E)$  is the usual Fermi function. The effects of Coulomb distortion on the electron

$$\begin{aligned} l^\mu \langle f | V_\mu | i \rangle &= \left[ a(q^2) \frac{\vec{P} \cdot \vec{1}}{2M} + e(q^2) \frac{\vec{q} \cdot \vec{1}}{2M} \right] \delta_{JJ'} \delta_{mm'} \\ &+ i \frac{b(q^2)}{2M} C_{J'1; J}^{m'k; m} (\vec{q} \times \vec{1})_k + C_{J'2; J}^{m'k; m} \left[ \frac{f(q^2)}{2M} C_{11; 2}^{nn'; k} l_n q'_n + \frac{g(q^2)}{(2M)^2} \vec{P} \cdot \vec{1} \left( \frac{4\pi}{5} \right)^{1/2} Y_2^k(\hat{q}) q^2 \right], \end{aligned} \quad (3a)$$

$$\begin{aligned} l^\mu \langle f | A_\mu | i \rangle &= C_{J'1; J}^{m'k; m} \frac{\epsilon_{ijk} \epsilon_{ij\lambda\eta}}{4M} \left[ C(q^2) l^\lambda P'^\eta - d(q^2) l^\lambda q'^\eta + \frac{h(q^2)}{(2M)^2} q^\lambda P'^\eta \vec{q} \cdot \vec{1} \right] \\ &+ C_{J'2; J}^{m'k; m} C_{12; 2}^{nn'; k} l_n \left( \frac{4\pi}{5} \right)^{1/2} Y_2^{n'}(\hat{q}) \frac{q^2}{(2M)^2} j_2(q^2) + C_{J'3; J}^{m'k; m} C_{12; 3}^{nn'; k} l_n \left( \frac{4\pi}{5} \right)^{1/2} Y_2^{n'}(\hat{q}) \frac{q^2}{(2M)^2} j_3(q^2), \end{aligned} \quad (3b)$$

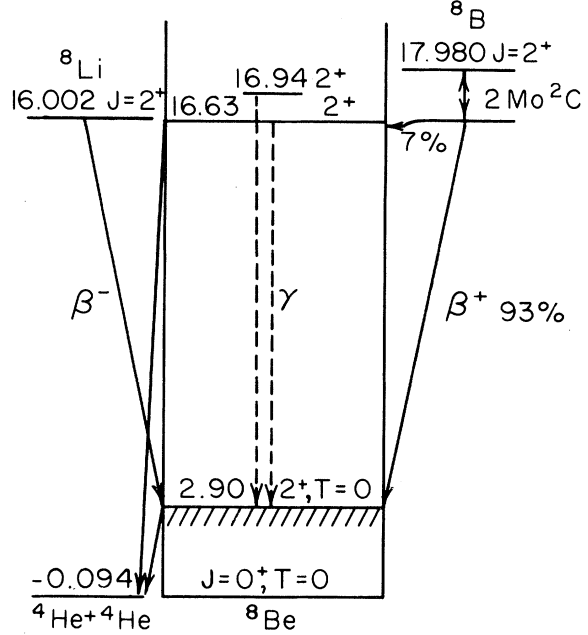


FIG. 1. Energy levels and relevant decays for  $A=8$  nuclei. The 16.63 and 16.94 MeV  $2^+$  states are nearly equally mixed in isospins  $T=0$  and  $T=1$ . The analogue  $M1$   $\gamma$ -decay width is therefore split between these two states.

wave function have been considered and are found to be small for the  $A=8$  decays.<sup>4,5</sup> The  $T$  matrix in Eq. (1), assuming the usual vector-axial vector form is,

$$T = \frac{G_V}{\sqrt{2}} \cos \theta_c \langle f | V_\mu(x) + A_\mu(x) | i \rangle l^\mu \quad (2)$$

where  $V_\mu(x)$  and  $A_\mu(x)$  are the nuclear vector and axial vector weak currents, respectively,  $G_V$  is the weak coupling constant,  $\theta_c$  is the Cabibbo angle, and  $l^\mu$  is the lepton weak current. We follow completely the format of Ref. 5 and only present the following to make the paper comprehensible. The vector and axial vector parts of  $T$  are defined up to second order in the recoil momentum as

TABLE I. Summary of the results of  $A = 8$   $\beta$  decay experiments.

Results from previous $\beta$ decay experiments in $A = 8$					
	${}^8\text{Li}$	${}^8\text{B}$		Ref.	
$\text{Log}(ft)$	5.61	5.64		7	
$\beta - \nu - \alpha$ ang. correl. coef. <sup>a</sup>	$-1.01 \pm 0.07$	...		9	
$\beta - \nu - \alpha$ ang. correl. coef.	$-0.88 \pm 0.08$	...		10	
$\beta$ asymmetry <sup>b</sup>	$0.08 \pm 0.01$	...		11	
$\beta - \alpha$ angular correlation measurements					
Reference	Nuclide	$E$ (MeV)	$a/E$ ( $\times 1000$ )	$p/E$ ( $\times 1000$ )	Ref.
Nordberg <i>et al.</i>	${}^8\text{Li}$	5	$-7.3 \pm 1.1$	$2.3 \pm 1.0$	12
	${}^8\text{Li}$	8	$-7.2 \pm 1.1$	$3.3 \pm 1.0$	
	${}^8\text{Li}$	11	$-8.7 \pm 0.7$	$3.16 \pm 0.6$	
	${}^8\text{B}$	11	$-8.7 \pm 0.9$	$-3.86 \pm 1.0$	
$p_- - p_+ = (0.007 \pm 0.0012)E$					
Eichner <i>et al.</i>	${}^8\text{Li}$	6.6	$-9.7 \pm 0.7$	$3.1 \pm 0.3$	9
	${}^8\text{B}$	7.0	$-11.1 \pm 1.3$	$-2.3 \pm 0.3$	
$p_- - p_+ = (0.0054 \pm 0.0004)E$					
Energy dependent slope of ( $ft$ ) asymmetry			$(1.0 \pm 5.7) \times 10^{-4} \text{ MeV}^{-1}$		8

<sup>a</sup> Neglecting energy dependent induced terms, the parameter  $b$  quoted above would be  $b = -1.0$  for a pure Gamow-Teller transition.

<sup>b</sup> The parameter quoted is not the asymmetry parameter but a quantity related to the channel spin of the compound ( ${}^7\text{Li} + n$ ) system. The interpretation of the parameter depends on both the channel spin and type of  $\beta$  decay (i.e., Fermi and/or Gamow-Teller).

where, with  $M_1$  and  $M_2$  the parent and daughter masses,  $M = \frac{1}{2}(M_1 + M_2)$ ,  $\vec{P} = \vec{p}_1 + \vec{p}_2$ , and  $\vec{q} = \vec{p}_1 - \vec{p}_2 = \vec{p} + \vec{k}$ . The  $C_{j_1 j_2 j_3}^{m_1 m_2 m_3}$ 's are vector-addition coefficients expressing the over-all conservation of angular momentum between the initial and final states and the weak fields.

Ten invariant form factors are introduced in Eqs. (3a) and (3b). Several of these are well known at zero momentum transfer and are termed Fermi  $a(0)$ , Gamow-Teller  $c(0)$ , while in recoil order one has weak magnetism  $b(0)$ , induced tensor  $d(0)$ , induced scalar  $e(0)$ , and pseudoscalar  $h(0)$ . Terms that enter Eqs. (3) of order  $q^2$ , are the second forbidden vector ( $f$  and  $g$ ) and second forbidden axial vector ( $j_2$  and  $j_3$ ).

Symmetry considerations however place important restrictions on these invariant form factors. Time reversal invariance requires that all these form factors be relatively real. Taking the weak vector current to be divergenceless (CVC) requires for transitions between states that are not members of the same isospin multiplet that the following relationships hold<sup>5</sup>:

$$a(q^2) = -\frac{1}{2M\Delta} q^2 e(q^2), \quad (4a)$$

$$g(0) = -\sqrt{\frac{2}{3}} \frac{2M}{\Delta} f(0), \quad (4b)$$

and  $b^2(0)$  is directly related to the radiative width

of the analogous isovector  $M1$  decay in  ${}^8\text{Be}$ . In addition, CVC requires that the second class part of any vector form factor must vanish. The classification of weak currents into first and second class was first carried out by Weinberg.<sup>13</sup> He showed that the  $G$  parity of the hadronic weak current associated with each of the form factors is ( $\pm 1$ ) for transitions within the same isospin multiplet. Those induced vector currents that have the same  $G$  parity as the recoil independent vector current ( $\gamma_\mu$ ) are termed first class as are those induced axial currents that have the same  $G$  parity as ( $\gamma_\mu \gamma_5$ ). Thus

$$G V_\mu G^{-1} = [V_\mu^I - V_\mu^{II}], \quad (5a)$$

$$G A_\mu G^{-1} = -[A_\mu^I - A_\mu^{II}], \quad (5b)$$

where  $V_\mu$  and  $A_\mu$  stand for the  $\mu$ 'th component of the vector and axial-vector currents, respectively. The Roman numeral denotes the class of the current, while the sign in brackets denotes the  $G$  parity of the second class current. If the transition is not within the same multiplet there can be first and second class contributions to each of the form factors.<sup>5</sup> However, they can be sorted with respect to their class measuring mirror decays to a common final state and combining results to extract either the first or second class part of a given form factor.

For the decays studied in the  $A = 8$  system in

this paper, the transitions are not within a common isospin multiplet and so we obtain our information by measuring the  ${}^8\text{Li}(2+T=1) \rightarrow {}^8\text{Be}(2+T=0)$  decay and the mirror decay  ${}^8\text{B}(2+T=1) \rightarrow {}^8\text{Be}(2+T=0)$ . In this decay  $a(0) \ll 0.01$  and as  $h(0)$  is multiplied by  $(m_e/8m_p)^2$  their contributions are ignored. The remaining form factors could in principle all have first and second class contributions but we shall respect CVC and only allow the axial currents to be second class. Accordingly we will treat  $c = c_{11} \pm c_{11}$  and  $d = d_{11} \pm d_{11}$ .

All of the above treatment is model independent. However, it is useful to try to relate the observed phenomenon to properties associated with free nucleons. To accomplish this the impulse approximation must be employed and nonrelativistic reductions of the operators obtained. This leads to the following expression<sup>5</sup> for the relevant form factors:

$$b = A \left[ g_v \langle f \| \sum_j \tau_j \vec{L}_j \| i \rangle + (g_v + g_m) \langle f \| \sum_j \tau_j \vec{\sigma}_j \| i \rangle \right], \quad (6a)$$

$$f = \sqrt{\frac{2}{3}} M \Delta g_v \left( \frac{4\pi}{5} \right)^{1/2} \langle f \| \sum_j \tau_j r_j^2 Y_2(\hat{r}) \| i \rangle, \quad (6b)$$

$$g = -\frac{4}{3} M^2 g_v \left( \frac{4\pi}{5} \right)^{1/2} \langle f \| \sum_j \tau_j r_j^2 Y_2(\hat{r}) \| i \rangle, \quad (6c)$$

$$f(E) = c^2 - \frac{2}{3} \frac{E_0}{M} [c^2 \pm cb + cd] + \frac{2}{3} \frac{E}{M} (5c^2 \pm 2cb) - \frac{1}{3} \frac{(m_e)^2}{ME} [2c^2 \pm 2cb + cd], \quad (8a)$$

$$g(E) = \frac{-2c^2 E}{Mv^*}, \quad (8b)$$

$$h(E) = \frac{E}{M} \left\{ \frac{1}{2} [c^2 \pm cb - cd] - \frac{1}{\sqrt{14}} \left[ \pm \sqrt{\frac{3}{2}} Cg \frac{(E_0 - E)}{2M} \pm \frac{3}{2} cf + 3cj_2 \frac{(E_0 - 2E)}{4M} \right] - \frac{3}{2\sqrt{35}} cj_3 \frac{E}{M} + \frac{(E + 2E_0)c^2}{2M(v^*)^2} \right\}, \quad (8c)$$

where  $v^*$  represents the velocity of the decay  $\alpha$  particle in the center of mass. The upper (lower) sign refers to electron (positron) decay. Time reversal invariance was assumed for the form factors in Eqs. (8).

The leading term in the spectral function  $f(E)$  is the form factor associated with the allowed axial vector transition  $c^2$ . Assuming for the present that  $c_{11} = 0$  and  $c_{11} \equiv c$ , the angular correlation between the charged lepton and the decay  $\alpha$  particles is of the form  $\omega_{\pm}(\theta_{\beta-\alpha}) \equiv 1 + a_{\pm} \cos \theta_{\beta-\alpha} + b_{\pm} \cos^2 \theta_{\beta-\alpha}$ , where

$$a \approx \frac{g(E)}{c^2} = -\frac{2E}{Mv^*} \quad (9a)$$

and

$$b \approx \frac{h(E)}{c^2} = \frac{E}{2m_n} \left\{ \frac{1}{A} \pm \frac{b}{Ac} - \frac{d}{Ac} \mp \sqrt{\frac{3}{28}} \frac{g}{A^2 c} \frac{(E_0 - E)}{m_n} \mp \frac{3}{\sqrt{14}} \frac{f}{Ac} - \frac{3}{\sqrt{14}} \frac{j_2}{A^2 c} \frac{(E_0 - 2E)}{2m_n} - \frac{3}{\sqrt{35}} \frac{j_3}{A^2 c} \frac{E}{m_n} + \frac{(E + 2E_0)}{A^2 m_n (v^*)^2} \right\}. \quad (9b)$$

Equation (9a) shows that the  $\cos \theta$  coefficient depends only upon  $v^*$  and  $E$ , and should be similar for the two decays. Utilizing the  $G$  parity character of the hadron current the following linear combinations of form factors may be extracted from the two ( $\beta^{\pm}$ ) angular correlations:

$$c \approx g_A \langle f \| \sum_j \tau_j \vec{\sigma}_j \| i \rangle, \quad (6d)$$

$$d_{11} \approx A g_A \langle f \| \sum_j \tau_j \vec{\sigma}_j \times \vec{L}_j \| i \rangle, \quad (6e)$$

$$j_k = -\frac{2}{3} M^2 g_A \left( \frac{4\pi}{5} \right)^{1/2} \langle f \| \sum_j \tau_j [\vec{\sigma}_j \cdot \vec{Y}_2(r_j)]^k \| i \rangle, \quad (6f)$$

where  $\Delta = M_1 - M_2$ ,  $g_v = 1$  and  $g_A = 1.23$ ,  $g_m = 3.7$  and is the anomalous part of the isovector nuclear moment. The second class induced tensor form factor  $d_{11}$  does not have an unambiguous impulse approximation prediction and therefore is not included in Eqs. (6).<sup>14</sup>

In terms of the invariant form factors the spectrum for the  $\beta$ - $\alpha$  correlation in  $A = 8$  is found to be<sup>5</sup>

$$dw = \frac{F_{\mp}(Z, E) G_v^2 (\cos \theta_c)^2 (E_0 - E)^2 p E dE d\Omega_e d\Omega_{\alpha}}{(2\pi)^5} \times \left\{ f(E) + g(E) \frac{\hat{K} \cdot \vec{p}}{E} + h(E) \left[ \frac{(\hat{K} \cdot \vec{p})^2}{E^2} - \frac{1}{3} \frac{p^2}{E^2} \right] \right\}, \quad (7)$$

where  $\hat{K}$  is a unit vector in the direction of the  $\alpha$  particle,  $E$  is the electron energy, and  $E_0$  is the end point energy. The spectral functions  $f(E)$ ,  $g(E)$ , and  $h(E)$  are given by

$$\delta_{-} = \rho_{8\text{Li}} - \rho_{8\text{B}} = \frac{E}{m_n} \left[ \frac{b}{Ac} - \frac{d_{11}}{Ac} - \sqrt{\frac{3}{28}} \frac{g}{A^2 c} \frac{E_0 - E}{m_n} - \frac{3}{\sqrt{14}} \frac{f}{Ac} \right]. \quad (10a)$$

$$\delta_+ = p_{8\text{Li}} + p_{8\text{B}}$$

$$= \frac{E}{m_n} \left[ \frac{1}{A} - \frac{d_1}{Ac} - \frac{3}{\sqrt{14}} \frac{j_2}{A^2 c} \frac{(E_0 - 2E)}{2m_n} - \frac{3}{\sqrt{35}} \frac{j_3}{A^2 c} \frac{E}{m_n} + \frac{(E + 2E_0)}{A^2 m_n (v^*)^2} \right]. \quad (10b)$$

Equations (10a) and (10b) show both linear and quadratic  $\beta$  energy dependence in  $\delta_+$ . This energy dependence is most useful in allowing one to determine the size of the "second forbidden" contributions to  $\delta_-$  and  $\delta_+$ . Assuming that CVC is valid, the form factor  $g$  in  $\delta_-$  can be related to an isovector ( $E_2$ )  $\gamma$  transition in  $^8\text{Be}$  and thereby provide a limit for the  $E^2$  dependence. It is important to note that  $\delta_-$ , Eq. (10a), contains both the weak magnetism and second class axial vector current form factors as the  $G$  parity of both these currents is the same. Hence to establish the existence of second class currents one must know the size of the weak magnetism form factor. If the analogous isovector  $M1$  radiative width is known, then CVC may be used to provide the value of the weak magnetism form factor.

A nonzero  $\delta_+$ , Eq. (10b) would indicate that some or all of the form factors  $d_1$ ,  $j_2$ , and  $j_3$  are contributing to the  $\beta$  decay rate. No direct measurement of these form factors in allowed nuclear  $\beta$  decay has been previously made.

### III. EXPERIMENT

The short lifetimes of  $^8\text{Li}$  and  $^8\text{B}$  require that they be produced and their decays be detected on line at an accelerator. Therefore the apparatus was designed to incorporate a source production chamber and a detection chamber connected through a small volume as shown in Fig. 2 that allowed for transport of the source target. This arrangement ensured identical detection geometries for the  $^8\text{Li}$  and  $^8\text{B}$  decays, even though the source production techniques differed slightly. Both experiments were carried out with beams supplied by the Brookhaven National Laboratory (BNL) 3.5 MeV Van de Graaff accelerator.

$^8\text{Li}$  was produced with the reaction  $^7\text{Li}(d,p)^8\text{Li}$  which has a  $Q = -0.192$  MeV. Targets consisted of  $60 \mu\text{g}/\text{cm}^2$  LiF (natural Li) evaporated onto a  $200 \mu\text{g}/\text{cm}^2$  Ni backing.  $^{19}\text{F}$  represented a possible source of unwanted  $\beta$  activity through the reaction  $^{19}\text{F}(d,p)^{20}\text{F}$  which has a  $Q = +4.38$  MeV.  $^8\text{Li}$  yield measurements over a range of deuteron beam energies from 0.7 to 1.8 MeV indicated a maximum at  $E_d = 0.8$  MeV. At this low bombarding energy, no detectable  $^{20}\text{F}$  activity was created. A 100 nA, 0.8 MeV deuteron beam produced counting rates of 200 counts/sec in each of four  $\alpha$  detectors and

600 counts/sec in each of two  $\beta$  detectors with thresholds set at 0.350 and 2 MeV, respectively. The  $^8\text{Li}$  source size was defined by a 3.18 mm diam circular collimator on the incident beam.

$^8\text{B}$  is much more difficult to produce. The reaction  $^6\text{Li}(^3\text{He}, n)^8\text{B}$  which has a  $Q = -1.976$  MeV was employed. The  $^8\text{B}$  yield observed using a thick target increased monotonically as the  $^3\text{He}$  energy was increased up to the maximum available of 3.4 MeV. However the average  $^8\text{B}$  recoil energy from a 3.4 MeV  $^3\text{He}$  beam is the order of 1 MeV and the range corresponding to this energy would require a thick target backing to collect the activity. This backing would both distort the  $\alpha$  energy spectrum and cause source scattering for the  $\beta$  particles. In order to keep the source thickness sufficiently thin, a catcher foil scheme was employed to collect the  $^8\text{B}$  recoils. Targets were made by evaporating  $250 \mu\text{g}/\text{cm}^2$   $^6\text{LiF}$  (99.3% enriched in  $^6\text{Li}$ ) onto a  $250 \mu\text{g}/\text{cm}^2$  Ni backing. The targets were placed with the LiF facing the

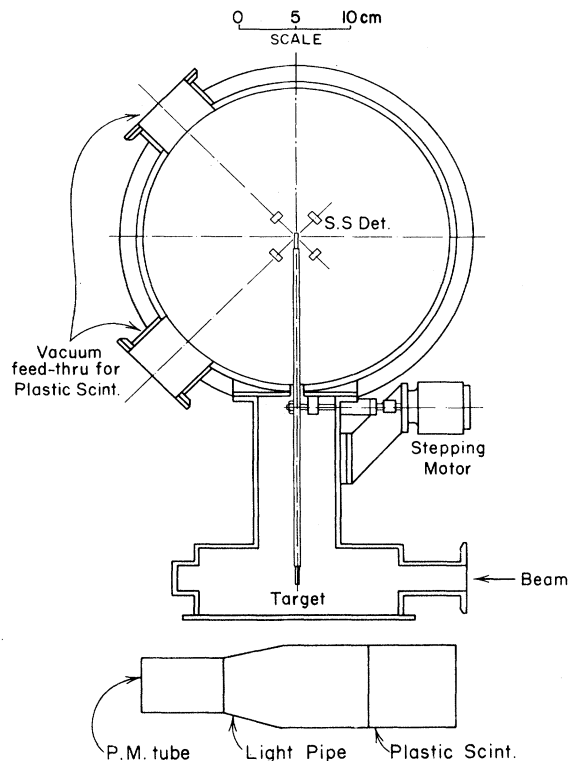


FIG. 2. Cross section of vacuum chamber geometry. The chamber had 36 cm vertical extent in order to allow the target rod to be rotated from the source production chamber to the detection chamber. The solid state detectors were mounted in thin Lucite holders. The electron energy loss was less than 40 keV through the detector-holder combination and the resulting small angle scattering was negligible.

beam to allow the backing to act as a degrader. The catcher foils were  $280 \mu\text{g}/\text{cm}^2$  Ni foils. Figure 3 shows the relative positions of the target, collimator, and catcher foil. An estimate of the scattering of the recoils in the degrader indicated the source size was 6.36 mm in diameter, as determined by the recoil collimator. A beam current of 450 nA produced 25 counts/sec in the  $\alpha$  detector and 250 counts/sec in the  $\beta$  detectors with the discriminator thresholds set as above. The quoted  $\beta$  detector rate includes both the real  $\beta$  events and the room background.

The vacuum chamber geometry is shown in Fig. 2. Two targets (or catcher foils) were used to effectively double the counting rate by simultaneously allowing source bombardment and counting. The targets were transported between the source production chamber and detection chamber by a Slo Syn stepping motor which moved in  $1.8^\circ$  steps. Rotating 100 steps ( $180^\circ$ ), as determined by a Preset Indexer, required 200 msec. The position accuracy quoted by the manufacturer was  $\pm 3\%$  per step (or  $\pm 0.17$  mm vertically) noncumulative. Measurements of the positioning accuracy over many cycles showed no vertical shift within the 0.4 mm accuracy of the measuring apparatus.

An array of four silicon surface barrier detectors and two plastic scintillators were used as particle detectors. The silicon detectors were transmission type surface barrier detectors of thicknesses varying between 50 and  $100 \mu$ . This thickness was sufficient to stop the most energetic  $\alpha$  particles (up to 8 MeV), while  $\beta$  rays would produce signals somewhat below the 0.3 MeV threshold. The noise widths varied between 25 and 45 keV. The  $\beta$  detectors consisted of a cylin-

der of Pilot B scintillator, 3.81 cm in radius by 7.62 cm in length, which was optically coupled to an ultraviolet transmitting acrylic light pipe. The light pipe was tapered from a radius of 3.81 to 2.54 cm and optically coupled to an RCA 8575 photomultiplier (PM) tube as shown in Fig. 2. This assembly was housed in a light tight container and connected to the detector chamber by an O-ring seal about the light pipe.

The detectors were arranged to determine  $\beta$ - $\alpha$  coincidence rates at nominal angles between the  $\beta$  and  $\alpha$  particles ( $\theta_{\beta\alpha}$ ) of  $0, 90, 180,$  and  $270^\circ$ . The two  $\beta$  detectors are  $90^\circ$  apart and thus determine coincidence rates for the same set of angles, but with each  $\alpha$  detector playing a different role. A lead collimator 1.25 cm thick was used to define the solid angle and reduce edge effects in the plastic scintillator.

The resulting detector half-angles were  $18^\circ$  and  $14^\circ$  for the  $\beta$  and  $\alpha$  counters, respectively. The relative positions of the  $\beta$  detectors,  $\alpha$  detectors, and lead shields are shown in Fig. 4. Detector position measurements, performed with the chamber evacuated, indicated small deviations from the nominal coincidence angles. These deviations were included in the data analysis, as indicated below.

A schematic of the electronic setup is shown in Fig. 5. The preamp outputs of the silicon detectors were fed into constant fraction discriminators for fast logic signals and into linear amplifiers for pulse height information. Lower level discriminators on the linear signals were set at 0.3 MeV as determined by a precision pulse generator, which was calibrated from a  $^{241}\text{Am}$   $\alpha$  source. The singles rates above this threshold for each of the four detectors were monitored in scalars to correct for

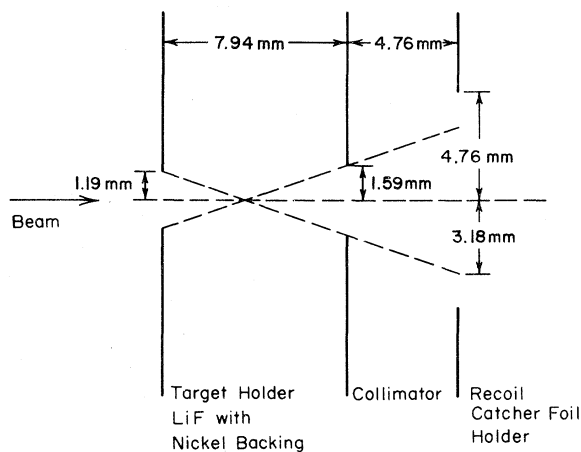


FIG. 3. Target and catcher foil geometry.  $^8\text{B}$  recoils were stopped in the catcher foil thus producing the  $^8\text{B}$  source.

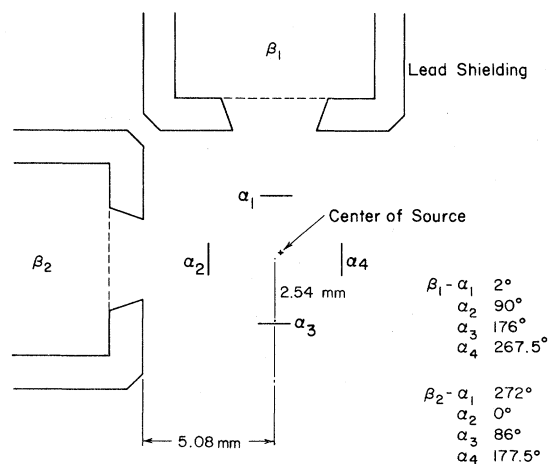


FIG. 4. Detector geometry. The coincidence angles listed were measured with the chamber evacuated.

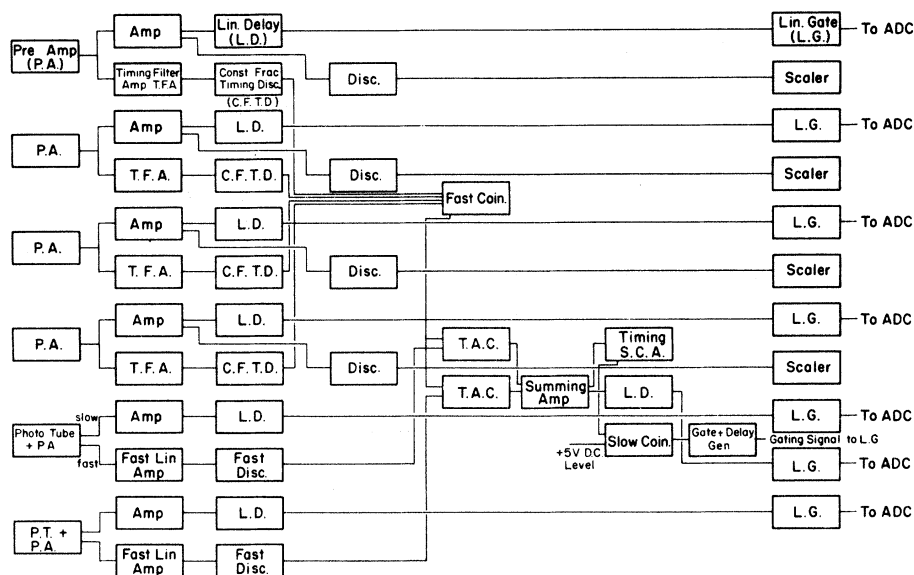


FIG. 5. The electronics utilized both slow and fast components to provide linear energy signals and timing information. Scalers measured singles  $\alpha$  rates to monitor the relative  $\alpha$  detector solid angles.

small differences in detector solid angle. The fast logic signals for the  $\beta$  detectors were taken off the PM anode and were sensed by a leading edge fast discriminator. The linear signals from the  $\beta$  detectors were taken from the ninth dynode of the PM which ensured linearity over the full range of  $\beta$  energies.

The experiment cycle time is more or less fixed by the  ${}^8\text{Li}$  and  ${}^9\text{B}$  lifetimes and was chosen to be 2 sec. The experiment was controlled by a crystal oscillator programmer, similar to the one designed by Schwender, Goosman, and Jones.<sup>15</sup> Four functions were governed by this programmer: (1) beam chopping (by pulsing a small vertical deflection magnet in the beam line); (2) actuating the preset indexer of the Slo-Syn motor to rotate the targets; (3) gating scalers; (4) providing a +5 V d.c. level for coincidence gating the ADCs (analog-to-digital converters) (see Fig. 5). The target-source exchange was completed in 0.4 sec during which time both scalers and ADCs were gated off. The remaining 1.6 sec were used to simultaneously bombard one target while detecting and storing the  $\beta$ - $\alpha$  coincidence information from the other.

The data were event mode recorded (emr) with an analyzer system consisting of seven ADCs, a buffer tape controller, and a magnetic tape drive. Each of the eight possible types of coincidence events was redundantly tagged by its ADC location and its associated time-to-amplitude converter (TAC) signal. The complete data analysis was carried out from the EMR tapes at the Princeton University Computer Center.

#### IV. DATA ANALYSIS AND EXPERIMENTAL RESULTS

The experimental data consisted of analog signals corresponding to  $\beta$  energy,  $\alpha$  energy, and a time interval between these signals that were digitized and event mode recorded. In the initial phase of analysis, criteria were established to define a valid event. The data were then grouped into  $\beta$  energy spectra and the correlation coefficients extracted as a function of  $\beta$  energy. Possible systematic errors were studied in detail in order to understand their effect on the data.

##### TAC spectra

Each  $\beta$  detector could be in coincidence with the four  $\alpha$  detectors. To determine the time interval between  $\beta$ - $\alpha$  events, two TAC were employed. Each  $\beta$  detector starts a TAC, while each of the discriminators sensing the  $\alpha$  events is connected to the TAC stop via different lengths of cable. Thus the pulse height of the signal from the TAC serves to uniquely determine the  $\beta$ - $\alpha$  pair that are in coincidence provided the accidental coincidence rate is negligible, as is the case at hand. The outputs of the two TACs are summed, hence a single ADC can store all the timing information in the experiment. A typical spectrum is shown in Fig. 6. The timing resolution, which varied between 3.2 and 6.5 nA, was quite adequate to keep the number of accidental coincidences occurring in the final data to less than 0.1%. An upper limit of the error due to this uncertainty was set at 1%

of the angular correlation coefficients.

With the experimental arrangement described above, valid coincidence events could occur between a  $\beta$  ray and two  $\alpha$  particles detected simultaneously at 0 and 180°, or, equivalently, at 90 and 270°. Such double events would have only one TAC signal associated with the detector (0°, 90°) providing the earliest stop signal. It is not possible to distinguish valid double events from random double events when the TAC signal occurred with the 0 or 90° detector. The number of random events, however, can be determined by counting how many  $\alpha$  particles from the 0°  $\alpha$  detector occurred with TAC signals from the 180°  $\alpha$  detector. The random rates were approximately 1% for the  ${}^8\text{Li}$  decay and less than 0.3% for the  ${}^8\text{B}$  decay. In order to correct for this systematic bias, half of the data was taken as indicated above, while for the other half, the timing roles of the 0°–180° and 90°–270°  $\alpha$  detector pairs were reversed. This reduces the uncertainty due to this count rate effect to a level estimated at 1% in the determination of the angular correlation coefficients for the  ${}^8\text{Li}$  decay and less than 0.25% for the  ${}^8\text{B}$  decay.

#### $\alpha$ spectra

The  $\alpha$  decay from the breakup of the  $2^+$ , 2.90 MeV level in  ${}^8\text{Be}$  is characterized by a mean energy of approximately 1.5 MeV, a half-width of approximately 1 MeV, and a high energy tail which extends nearly 5 MeV above the mean energy. A typical spectrum is shown in Fig. 7. A precision pulse generator, calibrated at 5.47 MeV by a  ${}^{241}\text{Am}$   $\alpha$  source, was used to set lower level cutoffs and

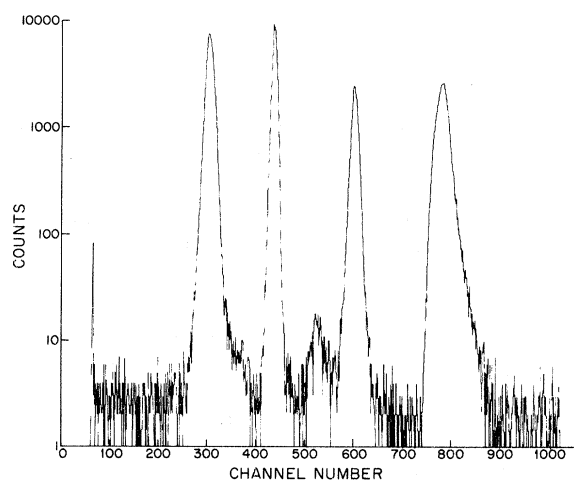


FIG. 6. TAC spectrum from one  $\beta$ - $\alpha$  detector array. Cable delays of 50, 100, and 150 nA were added to three of the four  $\alpha$  detectors. The tials are associated with a time walk for low energy  $\alpha$  particles.

to establish the  $\alpha$  spectra energy calibration. The  ${}^{241}\text{Am}$  source was mounted on a retractable rod inside the detector chamber and could be positioned in front of the  $\alpha$  detector without disturbing the detector geometry. The detectors were checked periodically throughout the experiment for gain shifts and drifts in the lower level discriminators. As we noted above, the singles rates from the four  $\alpha$  detectors were used to correct for differences in detector solid angle. The lower level cutoffs were set at the nominal value of 0.350 MeV. An error of  $\pm 50$  keV (lower level set at 0.400 MeV) would correspond to a 0.3% error in the measured singles rates. Drifts in the lower level cutoffs were measured to be less than  $\pm 25$  keV throughout the experiment. The corresponding uncertainty in the angular correlation coefficients was set at 3% for both  ${}^8\text{Li}$  and  ${}^8\text{B}$  decays.

Several effects cause energy shifts in the coincidence  $\alpha$  spectra as a function of  $\beta$ - $\alpha$  angle. One source of such shift is the  ${}^8\text{Be}^*$  recoil direction. A nonrelativistic calculation approximates the shift in the alpha energy as

$$E_{\alpha} = E_{\alpha'} - \left( \frac{7E_{\beta}}{6} - \frac{E_0}{6} \right) \left( \frac{E_{\alpha'}}{2m_{\alpha}c^2} \right)^{1/2} \cos\theta_{\beta-\alpha}, \quad (11)$$

where  $E_{\alpha'}$  is the center of mass  $\alpha$  energy,  $E_{\beta}$  is the  $\beta$  energy,  $E_0$  is the end point energy, and  $E_{\alpha}$  is the measured  $\alpha$  energy. Using an average  $E_{\beta}$ , and  $E_{\alpha'} = 1.5$  MeV, Eq. (11) predicts an increase of approximately 76 keV between  $\alpha$  particles at coincidence angles of 0 and 90°, and a further 76 keV shift between 90 and 180°. The experimental kinematic shift was found to be 70 keV. Another

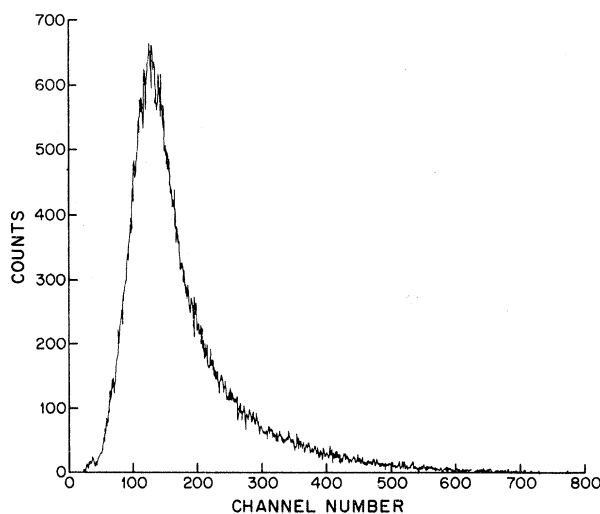


FIG. 7. A coincidence  $\alpha$  spectrum from  $\theta_{\beta\alpha} = 90^\circ$ . The peak occurs at 1.5 MeV and the tail extends up to nearly 6 MeV.

source of energy shift in the  $\alpha$  spectra is the energy loss in the source. This effect can be observed in the noncoincident spectra and was observed to differ between the detectors facing the front and back side of the target. It also differed for the  ${}^8\text{Li}$  and  ${}^8\text{B}$  decays because of the different techniques used to produce the sources. Lower level cutoff corrections for the two effects above were applied to the coincidence  $\alpha$  data in a region which contained few counts. An error of 50 keV in the shift analysis therefore corresponded to less than 0.1% error in the number of coincidence counts. The error estimate due to the coincidence  $\alpha$  spectra cutoffs was set at 1% of the correlation coefficients for both decays.

#### $\beta$ spectra

The angular correlation coefficients reported below are given as a function of  $\beta$  energy. This required an energy calibration of the  $\beta$  spectra. Since the  $\beta$  decay in this case is to a broad final level, the  $\beta$  spectra did not exhibit the usual allowed shape. Kurie plots are therefore not useful to establish a calibration. A previous<sup>6</sup> magnetic spectrometer measurement of the  ${}^8\text{Li}$  decay provided calibrations at the  $\frac{1}{2}$  max and  $\frac{1}{10}$  max points for the  ${}^8\text{Li}$  spectrum.  $\beta$  decays from  ${}^{20}\text{F}$  and  ${}^{16}\text{N}$  were also measured to check the detector linearity and establish the calibration. The sources were produced with a 1.5 MeV deuteron beam by the reactions  ${}^{19}\text{F}(d, p){}^{20}\text{F}$  and  ${}^{15}\text{N}(d, p){}^{16}\text{N}$ . The end point energies extracted were 5.41 MeV for the  ${}^{20}\text{F}$  decay and 10.4 and 4.36 MeV for the  ${}^{16}\text{N}$  decay. These three energies were compared to the  $\frac{1}{2}$  max and  $\frac{1}{10}$  max point from the  ${}^8\text{Li}$  spectrum. Deviations from a linear calibration were less

than 5% for all of the energies measured.

A spectrum shape for the  ${}^8\text{Li}$  decay was calculated and compared to the experimental shape in order to check both the  $\beta$  spectra and the calibration. The spectrum shape was found from the integrated three body phase space, without recoil, but corrected for Coulomb distortion. The number of counts as a function of  $\beta$  energy is

$$N(E) = F(Z, E)pE(E_0 - E)^2, \quad (12)$$

where  $E_0$  is the end point energy and  $F(Z, E)$  is the usual Fermi function. A set of allowed shapes was generated corresponding to the continuous distribution of end point energies in the  ${}^8\text{Li}$  decay. Each end point energy was weighted with the corresponding number of counts from the  $90^\circ$   $\alpha$  spectrum. A resolution of 10% was folded into the spectrum shape to account for the finite resolution of the detector. The resulting shape factor is compared to the  ${}^8\text{Li}$  spectrum in Fig. 8. The same procedure was applied to the positron spectrum from the  ${}^8\text{B}$  decay. A Monte Carlo calculation of the effect of the 511 keV annihilation  $\gamma$  rays indicated that the positron energy signal would be increased by approximately 190 keV, independent of initial positron energies between 3 and 15 MeV. This effect was treated as a zero level shift for the positron energy spectra. A comparison of the positron spectrum to the generated spectrum shape is shown in Fig. 9. Based upon the calibration procedure outlined above, an uncertainty of 3% for  ${}^8\text{Li}$  and 4% for  ${}^8\text{B}$  was assigned to the  $\beta$  energy. This corresponds to a 3 and 4% uncertainty in the correlation coefficients for  ${}^8\text{Li}$  and  ${}^8\text{B}$ , respectively.

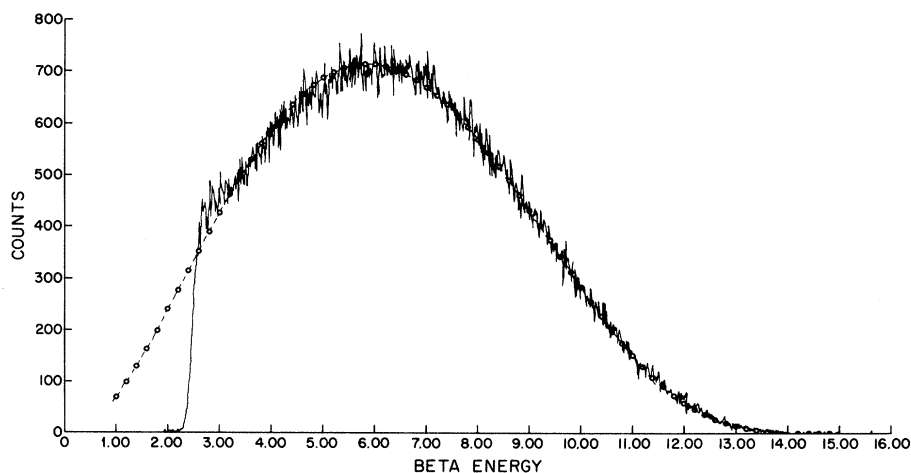


FIG. 8.  ${}^8\text{Li}$  coincidence  $\beta$  spectrum. The dashed line represents the phase space shape factor for an allowed decay, integrated over the  $\alpha$  decay spectrum. A 10% resolution factor was folded in to approximate the  $\beta$  detector resolution.

$\beta$  spectra, measured with detectors such as Si(Li) or plastic scintillators, can undergo distortions due to effects such as backscattering, bremsstrahlung, and, for positrons, annihilation in flight. Investigations of backscattering by Tillman<sup>16</sup> and Cambieri and Pappalardo<sup>17</sup> indicated that the backscattering coefficient(s) was  $\approx 0$  for an effective  $Z$  of 3 to 4. The effective  $Z$  for Pilot B is 4.5 which is in the region of small  $s$ . An upper limit of 5% was assigned to the backscattering coefficient for Pilot B. Further, the spectrum of backscattered electrons, calculated by Tillman, was relatively flat for low  $Z$  materials. This would correspond to a uniform distribution of energies for the backscattered events, up to the incident  $\beta$  energy. Monte Carlo calculations were used to simulate bremsstrahlung and positron annihilation processes. Estimates of these effects on the correlation coefficients were made, based upon the calculated energy spectra. The uncertainty due to the combined effects of backscattering and bremsstrahlung was estimated at 2% for  $^8\text{Li}$ . Including the positron annihilation

gave a 2.5% uncertainty for the  $^8\text{B}$  correlation coefficients.

#### Angular correlation coefficients

The observed coincidence rates are used to fix the coefficients of the expected angular correlation whose form is  $\omega(\theta) = 1 + a \cos \theta + b \cos^2 \theta$ . In order to extract  $a$  and  $b$ , corrections have to be applied for (1) finite detector solid angle, (2) finite source size and (3) actual detector coincidence angles. Integrating over both  $\alpha$  and  $\beta$  detector half angles gives the correlation, corrected for finite solid angle, as

$$\begin{aligned} \bar{\omega}(\theta) = & 1 + \frac{1}{3}b \left[ 1 - \frac{1}{2}\cos\alpha(1 + \cos\alpha)\frac{1}{2}\cos\beta(1 + \cos\beta) \right] \\ & + \frac{1}{4}a \cos\theta(1 + \cos\alpha)(1 + \cos\beta) \\ & + \frac{1}{4}b \cos^2\theta(\cos\alpha)(1 + \cos\alpha)(\cos\beta)(1 + \cos\beta), \end{aligned} \quad (13)$$

where  $\alpha$  and  $\beta$  are the  $\alpha$  and  $\beta$  detector half angles. The number of counts, normalized by the appropriate singles rate, at coincidence angle  $\gamma$  is

$$\begin{aligned} N(\gamma) = & 1 + \frac{1}{3}b \left[ 1 - \frac{1}{4}(\cos\alpha_\gamma \cos\beta_\gamma)(1 + \cos\alpha_\gamma)(1 + \cos\beta_\gamma) \right] + \frac{1}{4}a \cos\gamma(1 + \cos\alpha_\gamma)(1 + \cos\beta_\gamma) \\ & + \frac{1}{4}b \cos^2\gamma \cos\alpha_\gamma \cos\beta_\gamma (1 + \cos\alpha_\gamma)(1 + \cos\beta_\gamma) \\ = & C + aA_\gamma + bP_\gamma. \end{aligned} \quad (14)$$

For three angles  $\gamma$ ,  $\delta$ , and  $\rho$  the correlation coefficients are

$$a = \frac{N(\gamma)(P_\delta - P_\rho) + N(\delta)(P_\rho - P_\gamma) + N(\rho)(P_\gamma - P_\delta)}{N(\gamma)(A_\delta P_\rho - A_\rho P_\delta) + N(\delta)(A_\rho P_\gamma - A_\gamma P_\rho) + N(\rho)(A_\gamma P_\delta - A_\delta P_\gamma)}, \quad (15a)$$

$$b = \frac{N(\gamma)(A_\rho - A_\delta) + N(\delta)(A_\gamma - A_\rho) + N(\rho)(A_\delta - A_\gamma)}{N(\gamma)(A_\delta P_\rho - A_\rho P_\delta) + N(\delta)(A_\rho P_\gamma - A_\gamma P_\rho) + N(\rho)(A_\gamma P_\delta - A_\delta P_\gamma)}; \quad (15b)$$

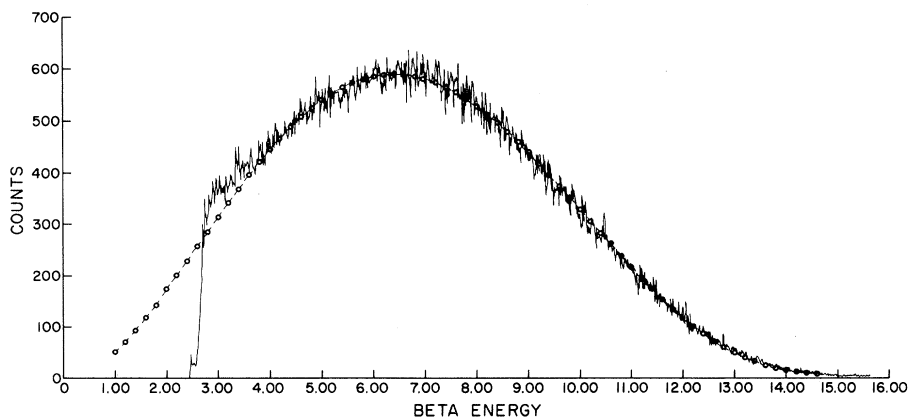


FIG. 9.  $^8\text{B}$  coincidence  $\beta$  spectrum. The calibration was corrected for the 0.511 MeV annihilation  $\gamma$  rays. The dashed line is the allowed shape factor for the  $^8\text{B}$  decay, with the 10% resolution factor folded in.

TABLE II. Correlation coefficients.

Energy	${}^8\text{Li}$		${}^8\text{B}$	
	$(a_- \times 1000)/E$	$(p_- \times 1000)/E$	$(a_+ \times 1000)/E$	$(p_+ \times 1000)/E$
4.9	$-7.92 \pm 0.20$	$3.55 \pm 0.87$	$-6.93 \pm 0.28$	$-3.32 \pm 0.86$
5.9	$-7.72 \pm 0.15$	$3.23 \pm 0.69$	$-6.76 \pm 0.21$	$-3.84 \pm 0.67$
6.9	$-8.09 \pm 0.13$	$3.25 \pm 0.58$	$-7.09 \pm 0.18$	$-4.75 \pm 0.55$
7.9	$-8.46 \pm 0.12$	$2.69 \pm 0.53$	$-7.56 \pm 0.16$	$-3.58 \pm 0.50$
8.9	$-8.36 \pm 0.12$	$3.42 \pm 0.52$	$-7.88 \pm 0.15$	$-5.01 \pm 0.49$
9.9	$-8.79 \pm 0.12$	$2.58 \pm 0.55$	$-8.30 \pm 0.15$	$-4.04 \pm 0.50$
10.9	$-9.34 \pm 0.14$	$3.18 \pm 0.62$	$-8.66 \pm 0.16$	$-4.66 \pm 0.54$
11.9	$-9.24 \pm 0.18$	$4.02 \pm 0.79$	$-8.89 \pm 0.20$	$-5.11 \pm 0.63$
12.9	$-9.78 \pm 0.26$	$4.29 \pm 1.16$	$-9.34 \pm 0.22$	$-4.96 \pm 0.82$

the actual detector angles and half angles were substituted into Eqs. (15a) and (15b) and the correlation coefficients were calculated. The solid angle corrections relied upon measurements of the experimental geometry. The uncertainty in these measurements led to assigning a 0.25% error to the  $\cos\theta$  coefficient and a 0.5% error to the  $\cos^2\theta$  coefficient.

A Monte Carlo calculation, modeled with the measured experimental geometry, was used to estimate the effect of the finite source size. An initial run with a point source verified the solid angle corrections calculated above. Two subsequent Monte Carlo runs were made for circular sources of 3.18 and 6.36 mm in diameter. The correction factors for the  $a$  coefficients were found to be (given as factors to multiply the uncorrected coefficients)  $1.04 \pm 0.005$  and  $1.02 \pm 0.005$  for 6.36 and 3.18 mm sources, respectively. The corrections for  $p$  were  $1.085 \pm 0.007$  and  $1.042 \pm 0.007$  again for the 6.36 and 3.18 mm sources. The errors quoted are statistical errors from the Monte Carlo calculation.

#### Experimental results

The data at coincidence angles of 90 and 270° represented redundant measurements. The final experimental results for each  $\beta$  detector array were found by averaging the 90 and 270° measurements. The results for the two  $\beta$  detectors were then added as two separate measurements. The resulting correlation coefficients are given in Table II. The systematic errors are summarized in Table III. The total error assigned to the correlation coefficients was found by adding the statistical and systematic errors in quadrature. The total error for  $\delta_\pm^0$  (see below) was obtained by adding in quadrature the average systematic errors for  ${}^8\text{Li}$  and  ${}^8\text{B}$ , excluding the geometry error, with the total statistical error. The total statistical error was found by considering the

determination of  $\delta_\pm^0$  at each  $\beta$  energy as a separate measurement and then combining the statistical errors of these separate measurements in quadrature. The geometry error was correlated between the two experiments since the same detector setup was used. Hence the geometry error for  $\delta_\pm^0$  was taken as the sum of the  ${}^8\text{Li}$  and  ${}^8\text{B}$  geometry errors and was added to the remaining error, while for  $\delta_\pm^{\pm}$  the geometry error canceled.

## V. DISCUSSION OF RESULTS

### Cos $\theta$ coefficient

The  $\cos\theta$  coefficient  $a$  is a predominantly kinematic term that depends upon the center-of-mass velocity of the  $\alpha$  particle. In Sec. II above we found that it was given approximately by

$$a \approx -\frac{2E}{Mv^*} \quad (16)$$

The approximation in Eq. (16) neglects the small energy dependent contributions to  $f(E)$  and the contribution from  $(-h(E)/3)$ . The correct form for  $a$  is

$$a = \frac{-2Ec^2}{Mv^*[f(E) - h(E)/3]} \quad (17)$$

where  $f(E)$  and  $h(E)$  are given in Eqs. (9a) and

TABLE III. Systematic errors.

Source of error	% correlation coefficient	
	${}^8\text{Li}$	${}^8\text{B}$
Coincidence $\alpha$ spectra	1	1
Singles $\alpha$ spectra	3	3
$\beta$ spectra calibration	3	4
$\beta$ spectra small effects	2	3.5
TAC spectra	1	1
Count rate	1	<0.25
Geometry-cos $\theta$	0.25	0.25
Geometry-cos $^2\theta$	0.5	0.5

(9c). In order to compare the experimental results to the predicted form for  $a$ , it is necessary to determine the average value of  $v^*$  in Eq. (17). Since the final state in  ${}^8\text{Be}^*$  is very broad,  $v^*$  cannot be a constant as a function of  $\beta$  energy. The quantity  $\langle 1/v^* \rangle$  must increase as the  $\beta$  energy increases since higher  $E_\beta$  require on the average a higher  $E_0$  and this in turn corresponds to a lower  $E_\alpha$ . The calculated values of  $\langle 1/v^* \rangle$  are obtained as follows. At a given  $\beta$  energy, the  $\alpha$  particle spectrum in coincidence at  $90^\circ$  corrected for target losses, is taken to minimize recoil distortion. Characterizing this observed  $\alpha$  spectrum as  $g(E_\alpha)$  where  $g(E_\alpha)dE_\alpha$  is the relative number of  $\alpha$  particles between  $E_\alpha$  and  $E_\alpha+dE_\alpha$ , the average value of  $\langle 1/v^* \rangle$  is calculated via

$$\left\langle \frac{1}{v^*} \right\rangle = \frac{\int 1/v_\alpha g(E_\alpha) dE_\alpha}{\int g(E_\alpha) dE_\alpha}. \quad (18)$$

The quantity  $\langle 1/v^* \rangle$  is calculated for  $3 \text{ MeV} \leq E_\beta \leq 13 \text{ MeV}$  by the procedure outlined above. As will be noted below, the largest energy dependent contribution to  $[f(E) - h(E)/3]$  is due to weak magnetism. Hence  $b$  was the only higher order form factor that was kept in the calculation of  $a$ .

The comparison of the theoretical predictions and the experimental results are shown in Fig. 10 for  ${}^8\text{Li}$  and Fig. 11 for  ${}^8\text{B}$ . Included in the figures are the three datum points (labeled with an  $N$ ) for  ${}^8\text{Li}$  and the single one for  ${}^8\text{B}$  from the experiment of Nordberg, Morinigo, and Barnes.<sup>12</sup> The two sets of data are in excellent agreement but in both

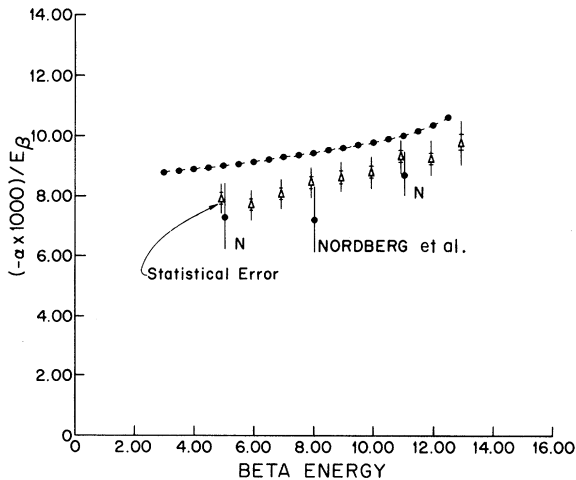


FIG. 10. Comparison of the  $\cos\theta$  coefficient for  ${}^8\text{Li}$  with the theoretical prediction. Three datum points from the experiment of Nordberg *et al.* (Ref. 12) are shown for comparison. The statistical error is flagged. The total error (statistical plus systematic) is indicated by the full error bar.

cases they fall 10–15% short of the theoretical prediction. Possible systematic effects were checked carefully, but no experimental or analysis errors have been found to date. Higher order contributions to the  $\cos\theta$  coefficient and contributions leading to a  $\cos^3\theta$  coefficient were calculated,<sup>18</sup> but could account for at most a 2% change in the theoretical prediction. It is still possible that experimental errors exist. However, at this time we are unable to account for this small discrepancy between the data and the theoretical result.

#### Weak magnetism and second class currents

We pointed out in Sec. II that the  $G$  parity of the form factors could be used to separate various combinations of induced terms. In particular, Eq. (10a) showed that the weak magnetism and second class induced tensor currents could be extracted by obtaining  $\delta_-$ . The Eq. (10a) for  $\delta_-$  was obtained assuming  $f(E) \approx c^2$ . The full expression for  $\delta_-$  is

$$\delta_- = p_{8\text{Li}} - p_{8\text{B}} = \left[ \frac{h(E)}{f(E) - h(E)/3} \right]_{8\text{Li}} \left[ \frac{h(E)}{f(E) - h(E)/3} \right]_{8\text{B}}. \quad (19)$$

The small terms that would enter into  $\delta_-$  as written in Eq. (19) require a change of sign between the two decays. They therefore must be products of terms that have opposite  $G$  parity. As a result of this restriction, their contribution to  $\delta_-$  is estimated to be at most 4%. Therefore it is assumed that only the four form factors  $b$ ,  $d_{\text{II}}$ ,  $f$ , and  $g$  contribute to  $\delta_-$ .

An independent determination of the second class induced tensor form factor  $d_{\text{II}}$  can be obtained

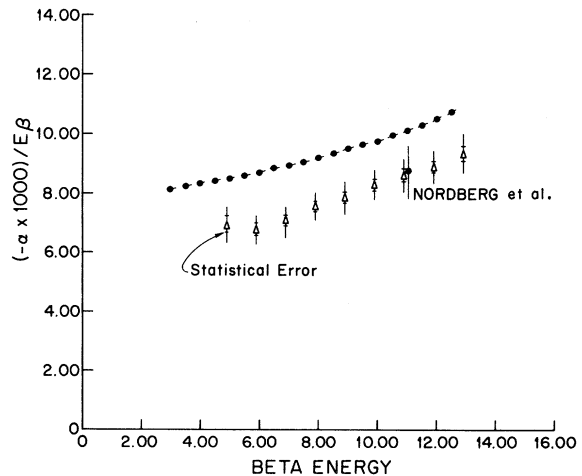


FIG. 11. Comparison of the  $\alpha$  coefficient for  ${}^8\text{B}$  with the theoretical prediction.

from the determination of the energy dependence of the  $ft$  asymmetry in mass 8. The results for the slope and intercept are reported in Table I. If we assume  $c = c_I \pm c_{II}$  and  $d = d_{II}$ , the  $ft$  asymmetry can be written as

$$\delta_{\text{sec}} = \frac{(ft)^+}{(ft)^-} - 1 \approx 4 \frac{c_{II}}{c_I} + \frac{E_0^+ - E_0^-}{M} \left( 2 \frac{c_{II}}{c_I} - \frac{2}{3} \frac{d_{II}}{c_I} \right). \quad (20)$$

The experimental result puts an upper limit on  $c_{II}$  of  $|c_{II}/c_I| < 0.025$ . Since this result is small,  $c_{II}/c_I$  can be neglected in the energy dependent part of the asymmetry. [We have assumed that  $C_{II}$  does not explicitly depend upon  $E_0$  in Eq. (20).] The experimental result which is quoted in Table I yields  $d_{II}/Ac = 0.14 \pm 0.8$ .

Our experimental values for  $\delta_- m_n/E_\beta$  as a function of  $E_\beta$  are shown in Fig. 12. To parametrize the additional energy dependence that could occur in this quantity via second forbidden effects we define

$$\delta_- = \delta_-^0 + E_\beta \delta_-^E. \quad (21)$$

A linear least squares fit to the data, using only the statistical error, yields  $\delta_-^0(m_n/E_\beta) = 5.7 \pm 1.3$  and  $\delta_-^E(m_n/E_\beta) = 0.2 \pm 0.14 \text{ MeV}^{-1}$  with a reduced  $\chi^2$  of 1.27. This result is consistent with negligible second forbidden contributions and as we estimate that these higher order effects should be small we feel justified in setting  $\delta_-^E = 0$ . With this condition the value of  $\delta_-^0$  becomes much better determined and we obtain  $\delta_-^0(m_n/E_\beta) = 7.0 \pm 0.3$  with a reduced  $\chi^2$  of 1.38, where the error is statistical. Including the systematic error we obtain  $\delta_-^0(m_n/E_\beta) = 7.0 \pm 0.5$ . It should be noted at this time that our results disagree somewhat with Eichner *et al.*<sup>9</sup> who obtained  $\delta_-^0(m_n/E_\beta) = 5.1 \pm 0.4$ , but we are in good agreement with Nordberg *et al.* who have measured  $6.6 \pm 1.2$ . The cause for the disagreement between the value reported in Ref. 9 and our work lies in the considerably smaller value obtained for  $p_+$ . There is insufficient experimental detail in Ref. 9 for us to further investigate the possible origin of the disagreement.

To proceed with a completely model independent investigation at this point would require that the isovector  $M1$  decay rate from the isospin mixed  $2^+$  levels in  ${}^8\text{Be}$  at 16.63 and 16.94 MeV be known. Assuming CVC to be true, and neglecting higher order terms that our data indicate to be small, one can write<sup>19</sup>

$$\Gamma_{1,1} = \left( \frac{b}{Ac} \right)^2 \frac{1}{m_n^2} \frac{E_\gamma^3}{3(137)} \frac{(ft)^{14} O}{(ft)}, \quad (22)$$

where  $\Gamma_{1,1}$  is the isovector  $M1$  width referred to above,  $f_0 t_{1/2}$  is the  $ft$  value for the allowed Gamow-Teller decay, and  $E_\gamma$  is the energy (in

MeV) of the  $\gamma$  ray emitted in the decay to the first excited state of  ${}^8\text{Be}$ . While there are some subtle problems associated with the actual determination of  $f_0 t_{1/2}$  and the appropriate value to take for  $E_\gamma$  because of the finite width of the final state it is instructive to use the values appearing in the literature.<sup>7</sup> Thus using  $f_0 t = 407, 360$  and  $E_\gamma = 14.00 \text{ MeV}$  yields

$$\Gamma_{1,1} = 2.9 \pm 0.4 \text{ eV}. \quad (23)$$

A sizable deviation of the radiative width from this value would indicate the presence of a  $d_{II}$  form factor or a breakdown of CVC. Experiments to measure this width are well underway and a number should be forthcoming soon.<sup>20</sup>

In the absence of this result the best to be done at present is to employ the impulse approximation and nuclear wave functions to calculate the expected value of the weak magnetism term. Four sets of nuclear wave functions were used to calculate the form factors  $b$ ,  $f$ , and  $g$ . The results of these calculations are shown in Table IV. The Nilsson model calculations assumed a deformation of  $\beta = 0.3$ , and the radial matrix elements have the value  $\langle r^2 \rangle = 4.44 \text{ fm}^2$ .<sup>21</sup> (Some phase errors were found in the previously reported results.<sup>22</sup> Therefore the matrix elements reported here differ slightly from those in the preceding publication, but all conclusions remain unchanged.) The calculations including second forbidden contributions are shown com-

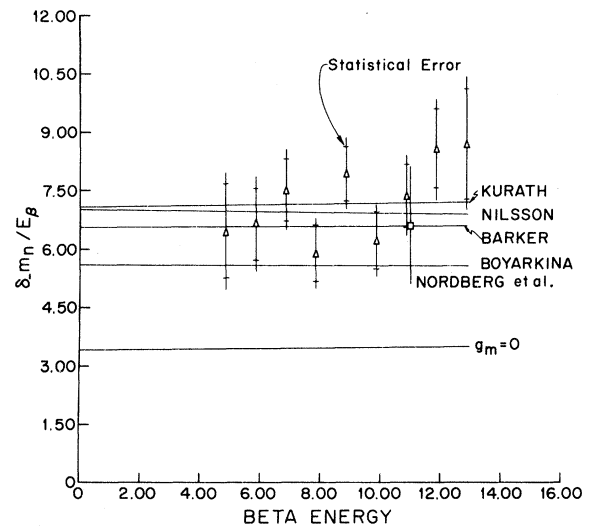


FIG. 12. Experimental results for  $(\delta_- m_n/E_\beta)$ . The four nuclear wave function predictions are in good agreement with the data. The CVC prediction  $g_m = 3.7$  was used for the four calculations. The effect of CVC is explicitly shown by plotting Barker's prediction with  $g_m = 0$ .

TABLE IV. Results employing nuclear wave functions to calculate form factors  $b$ ,  $f$ , and  $g$ .

Wave function	$\langle \Psi_f   \sum_j \tau_j^+ \vec{\sigma}_j   \Psi_i \rangle$	$\langle \Psi_f   \sum_j \tau_j^+ L_{zj}   \Psi_i \rangle$	$\langle \Psi_f   \sum_j \tau_j^+ Y_2(\hat{r}_j)   \Psi_i \rangle$ (fm <sup>2</sup> )	$\delta$	$\frac{b}{Ac}$	$\frac{d_{II}}{Ac}$
Barker <sup>a</sup>	+0.68	+2.24	-0.13	$\frac{E}{m_n} \left[ \frac{b}{Ac} - (0.003)(E_0 - E) + 0.05 \right]$	6.5	-0.5
Boyarkina <sup>b</sup>	-0.70	-1.48	-0.10	$\frac{E}{m_n} \left[ \frac{b}{Ac} + (0.002)(E_0 - E) - 0.04 \right]$	5.6	-1.4
Kurath <sup>c</sup>	-0.82	-2.94	+0.51	$\frac{E}{m_n} \left[ \frac{b}{Ac} - (0.008)(E_0 - E) + 0.16 \right]$	7.0	+0.0
Nilsson <sup>d</sup>	0.49	1.90	0.19	$\frac{E}{m_n} \left[ \frac{b}{Ac} + (0.004)(E_0 - E) - 0.09 \right]$	7.1	+0.1

<sup>a</sup> F. C. Barker, Nucl. Phys. S3, 418 (1966).  
<sup>b</sup> A. N. Boyarkina, Izv. Akad. Nauk SSSR Ser. Fiz. 28, 337 (1964) [Bull. Acad. Sci. USSR Phys. Ser. 28, 255 (1965)]. It is not clear to the authors how the parameters for the  $A=8$  wave functions were chosen by Boyarkina. However, since the wave functions are in the literature, their predictions have been included.  
<sup>c</sup> D. Kurath (private communication).  
<sup>d</sup> J. P. Davidson, *Collective Models of the Nucleus* (Academic, New York, 1968). The deformation parameter was chosen as  $\beta=0.3$ .

pared to the data in Fig. 12. As is evident from the figure the calculated effects of the second forbidden vector terms are negligible and the data support this. In this comparison the effect of CVC is reckoned by using the isovector anomalous magnetic moments of the nucleons and  $d_{II}$  is set equal to 0. The agreement between the wave function prediction and the data is remarkable and is seen consistent with  $d_{II}/Ac=0$ . In the calculation of  $\delta_-(m_n/E)$  all of the form factors but  $b$  appear to be small. The calculations are therefore only sensitive to  $\langle \|\sum_j \vec{L}_j \tau_j\| \rangle / \langle \|\sum_j \vec{\sigma}_j \tau_j\| \rangle$  and hence the good agreement should not be too surprising. The necessity of including CVC through  $g_m$  is pointed out explicitly by showing the results for Barker's wave functions with  $g_m=0$  in Fig. 12. Using the experimentally determined value of  $\delta_-(m_n/E_\beta) = 7.0 \pm 0.5$ , and the average value of the wave function calculation we find  $d_{II}/Ac = -0.45 \pm 0.8$ .

First class induced tensor

Equation (10b) above predicts  $\delta_+$  to depend on a first class induced tensor form factor ( $d_1$ ) and second forbidden axial vector form factors  $j_2$  and  $j_3$ . The experimental values for  $\delta_+(m_n/E)$  are shown in Fig. 13 with the trivial  $1/A^*$  and  $(E+2E_0)/A^2 m_n v^{*2}$  dependence indicated in Eq. (10b) taken out. Using the format of Eq. (21) a linear least squares fit to  $\delta_+(m_n/E)$  yields  $\delta_+^0(m_n/E) = -0.5 \pm 1.3$  and  $\delta_+^E m_n/E = 0.13 \pm 0.14$  MeV<sup>-1</sup> with a reduced  $\chi^2 = 0.30$ . In terms of the above form factors, these results correspond to  $[d_1/Ac + 0.006(j_2/A^2 c)] = 0.5 \pm 1.3$  and  $[-0.0009(j_2/A^2 c)$

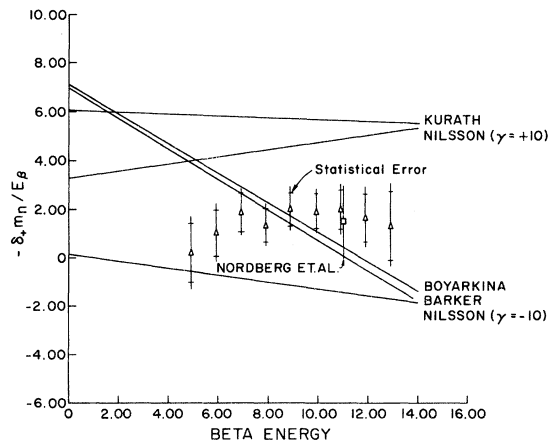


FIG. 13. Experimental results for  $(\delta_+ m_n/E_\beta)$ . The wave function predictions are in poor agreement with data and with each other. In this case, the wave function calculations are complicated because three matrix elements contribute significantly to the predicted result.

$+0.0005(j_3/A^2c)] = 0.13 \pm 0.14$ , where we have used  $E_0 = 13$  MeV. If no linear energy dependence is assumed to be present in the experimental determination of  $\delta_+^0(m_n/E)$  the result  $\delta_+^0(m_n/E) = -1.7 \pm 0.3$  is obtained with a reduced  $\chi^2 = 0.39$ . Including systematic errors gives  $\delta_+^0(m_n/E) = -1.7 \pm 0.5$ .

In order to unravel the contributions from the three form factors above ( $d_1$ ,  $j_2$ , and  $j_3$ ) the four sets of nuclear wave functions were employed to calculate  $d_1$ ,  $j_2$ , and  $j_3$ . The results of these calculations are presented in Table V. The calculations are compared to the experimental results in Fig. 13. Because of the large contribution from each term in the wave function predictions, it is not possible to eliminate any of the form factors in  $\delta_+$  and present a definitive result for a first class induced tensor current. The poor agreement between the wave function results and the experimental data may signal a breakdown of the impulse approximation for the second forbidden contributions. It has been pointed out previously that meson exchange effects could be important for the axial vector form factors.<sup>14</sup> However, careful study of second and third forbidden unique decay were found to be in good agreement with nuclear wave functions.<sup>21</sup> Attempts to see if "collective suppression"<sup>21</sup> would yield considerably smaller values for  $j_2$  and  $j_3$  showed this effect nowhere near large enough to bring the Nilsson model prediction into line.

We should note that the small contributions that were ignored in Eq. (11b) could account for a significant part of  $\delta_+$ . We have not considered these effects in detail, however, because of the obvious difficulties associated with the analysis of the experimental results. Further, even if one were to neglect the second forbidden terms, the small value observed for  $d_1/Ac$  is only consistent with the Nilsson model calculation. All the other models yield results that are a factor of 2 to 3 too large. There may well be a very important role being played by mesonic exchange effects,<sup>14</sup> but this is a most difficult hypothesis to investigate further.

### CONCLUSIONS

The relative consistency of our measurement of the quantity  $\delta_-(m_n/E)$  gives confidence that the recoil order term ( $b/Ac - d_{II}/Ac$ ) is well determined by the  $\beta^\pm - \alpha$  angular correlations without being obscured by higher order terms. The agreement of our result with impulse approximation wave function calculations is gratifying, particularly since all the models agree reasonably well. However, the weak magnetism part  $b/Ac$  should

TABLE V. Results employing nuclear wave functions to calculate  $d_1$ ,  $j_2$ , and  $j_3$ .

Wave function	$\langle \Psi_f \  \sum_f \tau_j^\pm \vec{\sigma}_j \times \vec{L}_j \  \Psi_i \rangle$	$\langle \Psi_f \  \sum_f \tau_j^\pm [\vec{\sigma}_j, \vec{Y}_2(r_j)]^2 \  \Psi_i \rangle$	$\langle \Psi_f \  \sum_f \tau_j^\pm [\vec{\sigma}_j, \vec{Y}_2(r_j)]^3 \  \Psi_i \rangle$	$\delta_+$	$\frac{d_1}{Ac}$
Barker	3.47	-5.06	9.29	$\frac{E}{m_n} \left[ \frac{d_1}{Ac} - 1.91 + 0.63E \right]$	5.10
Boyarkina	-3.42	6.71	-6.62	$\frac{E}{m_n} \left[ \frac{d_1}{Ac} - 2.23 + 0.61E \right]$	4.89
Kurath	-3.61	+5.39	7.59	$\frac{E}{m_n} \left[ \frac{d_1}{Ac} - 1.71 + 0.03E \right]$	4.41
Nilsson <sup>a</sup>	0.86	-0.30	-0.75	$\frac{E}{m_n} \left[ \frac{d_1}{Ac} + 1.59 + 0.14E \right]$	1.75

<sup>a</sup> The Nilsson model calculation requires a  $K$  band mixing parameter  $\gamma = (K=2)/(K=1)$ . The Gamow-Teller transition in  $A=8$  is hindered because only a small amount of  $K=1$  is mixed into the predominantly  $K=2$  initial state. Since the final state is  $K=0$ , the GT transition must proceed via the  $K=1$  admixture. However, the  $j_2$  and  $j_3$  matrix elements can go directly by the  $K=2$  component. The value  $\gamma = \pm 10$  was found based upon the  $\log(\beta')$  and the result for  $c$  in Table IV.

be fixed by the corresponding isovector  $M1$  decay in  ${}^8\text{Be}$  before undue conclusions are drawn about the validity of CVC or the absence of a second class interaction. Our use of the impulse approximation assumes that  $g_A$  also is not renormalized in the nucleus and there is not much strong evidence on this matter at the moment.<sup>23</sup>

Table I shows previously determined values for  $\delta_{\pm}^0(m_n/E_{\beta})$  along with those obtained from this work. Our results are seen to be in good agreement with Nordberg *et al.* and in severe disagreement with the more precise determination of Eichner *et al.* A closer look at these results show excellent agreement between these three groups<sup>9, 12, 24</sup> in the coefficients of the  ${}^8\text{Li}$   $\beta$ - $\alpha$  correlation but sizable disagreement with the Eichner *et al.*<sup>9</sup> on the  ${}^8\text{B}$   $\beta^+$ - $\alpha$  angular correlation. It may therefore be desirable to repeat the  ${}^8\text{B}$  experiment once again.

Before commenting on the values obtained for  $\delta_{\pm}^0(m_n/E_{\beta})$ , the small discrepancies that are occurring for the coefficient of the  $\cos\theta$  term should be pointed out. The nontrivial physics input (allowed  $\beta$ - $\nu$  correlation and the conservation of momentum) that determines this coefficient is so small that the 10% discrepancy that we presently have with its predicted value is disturbing. Particularly disturbing is the fact that our determination of  $a_{\pm}$  is in good agreement with most previous workers.<sup>12, 24</sup> It is probably worthwhile to further investigate this effect.

Our experimental determination of a value for  $\delta_{+}(m_n/E)$  agrees with that of the Cal Tech group<sup>12</sup> but is some five standard deviations from the value fixed by authors of Ref. 9. As the contribution to  $d_1$  comes from the timelike component of

$\gamma_{\mu}\gamma_5$ , its strength is in principle fixed by  $g_A(0)$  [see Eq. (6e)]. The predictions of the model wave functions for  $\delta_{+}(m_n/E)$  disagree with each other and with the experimental data. The apparent source of this disagreement is that they all predict the contribution of the second forbidden axial vector terms to be too large. The lack of energy dependence in our data would tend to make one believe that these terms are very small. However, even if these terms are neglected, only the Nilsson model which yields a value for  $d_1/Ac$  of 1.77 for  $\beta=0.3$  agrees with our experimental result. It is difficult to envision an experiment that can measure the second forbidden contributions directly; however, considerable light could be shed on the subject if one could fix the branch to the  ${}^8\text{Be}$  ground state. This decay must be second forbidden and this level has an intrinsic wave function that is quite similar to the  $2^+$  first excited state. If the second forbidden axial vector terms are as large as the models indicate, then the branch to  ${}^8\text{Be}$  ground state is approximately  $(3 \times 10^5)^{-1}$ .

#### ACKNOWLEDGMENTS

The authors would like to thank the Brookhaven National Laboratory for its hospitality and helpfulness in aiding our experimental effort. Of particular help were Dr. D. Alburger, Dr. M. Levine, Dr. L. Remsburg, and Mr. Edward Riley. Very useful discussions on the nature of and interpretation of the experiment were had with Professor F. Calaprice, Professor B. Holstein, and Professor S. Treiman.

†Work supported in part by the National Science Foundation.

\*Present address: Cyclotron Institute, Texas A&M University.

<sup>1</sup>C. S. Wu, *Rev. Mod. Phys.* **36**, 619 (1964); Y. K. Lee, L. W. Mo, and C. S. Wu, *Phys. Rev. Lett.* **10**, 253 (1963).

<sup>2</sup>D. H. Wilkinson, *Phys. Lett.* **31B**, 447 (1970).

<sup>3</sup>I. S. Towner, *Nucl. Phys.* **A216**, 589 (1973).

<sup>4</sup>B. R. Holstein and S. B. Treiman, *Phys. Rev. C* **3**, 1921 (1971); B. R. Holstein, *ibid.* **4**, 730, 764 (1970); **5**, 1529 (1972).

<sup>5</sup>B. R. Holstein, *Rev. Mod. Phys.* **46**, 789 (1974).

<sup>6</sup>W. F. Hornyak and T. Lauritsen, *Phys. Rev.* **77**, 160 (1950).

<sup>7</sup>F. Ajzenberg-Selove and T. Lauritsen, *Nucl. Phys.* **A227**, 1 (1974).

<sup>8</sup>D. H. Wilkinson and D. E. Alburger, *Phys. Rev. Lett.* **26**, 1127 (1971).

<sup>9</sup>H. Eichner, K. H. Lauterjung, H. Meinhardt, B. Schwimmer, and U. Schmidt-Rohr, *Z. Naturforsch.* **21A**, 908 (1966).

<sup>10</sup>W. Gruhle, K. H. Lauterjung, and B. Schwimmer, *Nucl. Phys.* **A74**, 139 (1965).

<sup>11</sup>Y. G. Abov, O. N. Yermakov, A. D. Gulko, P. A. Krupchitsky, and S. S. Trostin, *Nucl. Phys.* **34**, 505 (1962).

<sup>12</sup>M. E. Nordberg, Jr., F. B. Morinigo, and C. A. Barnes, *Phys. Rev.* **125**, 321 (1962).

<sup>13</sup>S. Weinberg, *Phys. Rev.* **112**, 1325 (1958).

<sup>14</sup>K. Kubodera, J. Delorme, and M. Rho, *Nucl. Phys.* **B66**, 253 (1973).

<sup>15</sup>G. E. Schwender, D. R. Goosman, and K. W. Jones, *Rev. Sci. Instrum.* **43**, 832 (1972).

<sup>16</sup>K. Tillmann, UCRL Report No. UCRL-19718, 1970 (unpublished).

<sup>17</sup>A. Cambieri and R. Papalardo, *Nuovo Cimento* **6**, 743 (1957).

<sup>18</sup>B. R. Holstein (private communication).

<sup>19</sup>M. Gell-Mann, Phys. Rev. 111, 362 (1958).

<sup>20</sup>A. Nathan, G. T. Garvey, P. Paul, and E. K. Warburton (private communication).

<sup>21</sup>E. K. Warburton, G. T. Garvey, and I. S. Towner, Ann. Phys. (N.Y.) 57, 174 (1970).

<sup>22</sup>R. E. Tribble and G. T. Garvey, Phys. Rev. Lett. 32, 314 (1974).

<sup>23</sup>D. H. Wilkinson, Phys. Rev. C 7, 930 (1973); Nucl. Phys. A209, 470 (1973); A225, 365 (1974).

<sup>24</sup>W. Gruhle, K. H. Lauterjung, B. Schwimmer, and U. Schmidt-Rohr, Nucl. Phys. 42, 321 (1963).